Imaging ClN_3 photodissociation from 234 to 280 nm

Peter C. Samartzis,*[a] Nils Hansen[b] and Alec M. Wodtke[a]

Received 1st March 2006, Accepted 27th March 2006
First published as an Advance Article on the web 7th April 2006
DOI: 10.1039/b603129c

We report $Cl(^2P_{3/2})$ and $Cl^*(^2P_{1/2})$ fragment images following ClN_3 photolysis in the 234–280 nm region measured by velocity map imaging. Kinetic energy distributions change shape with photolysis wavelength from bimodal at 234 and 240 nm to single peak at 266 and 280 nm. Where two peaks exist, their ratio is significantly different for Cl and Cl* fragments. The single peak of 266 and 280 nm and the faster peak at 234 and 240 nm are assigned to a Cl + linear-N_3 dissociation channel, in agreement with previous work. The slow peak in the bimodal distributions is assigned to the formation of a high energy form (HEF) of N_3. Candidates for the identity of HEF-N_3 are discussed. Combining our data with photofragmentation translational spectroscopy results, we determined the threshold for the appearance of HEF-N_3 at 4.83 ± 0.17 eV photolysis energy. This threshold behavior is similar to recently reported results on the wavelength dependence of HN_3 photolysis, where the threshold was associated with a ring closed isomer of HN_3 on the S_1 potential energy surface. We also note that the HEF-N_3 formation threshold observed for ClN_3 occurs where the energy available to the products equals the isomerization barrier from linear to cyclic-N_3.

Introduction

Cyclic-N_3 is the smallest closed ring in the group of nitrogen allotropes, many of which are theoretically predicted to be stable,[1] yet only five (linear N_3 isomer being one of them) have been experimentally observed. Recently, velocity map imaging (VMI) work on ClN_3 photolysis at 235 nm provided indirect evidence of cyclic-N_3 formation.[2] Cl atoms probed in those experiments exhibit a bimodal translational energy distribution with the higher translational energy peak corresponding to formation of Cl and linear N_3. The low translational energy peak characteristics match very well the theoretically predicted energetics[3–5] for the formation of cyclic-N_3. However there is no direct evidence on the structure of that N_3 form, so we refer to it as high energy form of N_3 (HEF-N_3).

These observations triggered a series of experiments on ClN_3. Photofragment translational spectroscopy (PTS) experiments using electron impact ionization to detect 248 nm ClN_3 photolysis fragments, showed that 95% ± 3% of ClN_3 dissociates *via* the Cl + N_3 channel[6] contrary to previous established knowledge that the channel leading to NCl + N_2 formation dominates the absorption. Furthermore, the Cl translational energy distribution from ClN_3 photodissociation at 248 nm exhibits a similar bimodality as seen in VMI experiments at 235 nm. As this technique relies on electron impact ionization, slow-channel N_3 fragments were detected directly, demonstrating that HEF-N_3 is stable enough to exist 100 μs after its production. However a large fraction of it undergoes dissociation to N_2 + N. That and other secondary photodissociation pathways of the fragments in those experiments were also explored.[7]

More evidence that HEF-N_3 must be significantly different from linear N_3 comes from PTS experiments using synchrotron radiation ionization to detect photofragments, again at 248 nm photolysis of ClN_3.[8] From the clearly resolved peaks of fast and slow N_3 fragments that were measured *vs.* ionization energy (*i.e.* tuning an undulator that controls the VUV wavelength), the ionization threshold of the HEF-N_3 was observed to be 10.67 ± 0.2 eV while the threshold[9] for the linear N_3 was confirmed once again to be at 11.07 ± 0.2 eV. The theoretically predicted ionization threshold for cyclic-N_3 (10.58 eV) is in good agreement with the observed threshold for HEF-N_3.[10] The energy resolution of those experiments was limited by the synchrotron radiation bandwidth.

Until now there is evidence for HEF-N_3 production at two wavelengths, 235 and 248 nm only. In the present paper we present the results of VMI experiments on the photolysis of ClN_3 at 234, 240, 266 and 280 nm and we combine those results with existing PTS data in an effort to determine how HEF-N_3 production depends on the photodissociation energy of its parent molecule. The study reveals a marked energetic threshold at 4.83 ± 0.17 eV, in the midst of the S_2–S_0 absorption system. These results are at least qualitatively similar to a recent[20] wavelength dependent study on HN_3, where theory could be successfully employed to identify the observed photodissociation threshold with a ring-closed HN_3 structure on the S_1 surface, presumably produced after S_2–S_1 surface hopping.

Experimental

For ClN_3 preparation, a 5% mixture of Cl_2 in He flows through moist cotton wool containing dispersed NaN_3. The

[a] *Department of Chemistry and Biochemistry, University of California Santa Barbara, Santa Barbara, CA 93106, USA. E-mail: sama@chem.ucsb.edu*
[b] *Combustion Research Facility, Sandia National Laboratories, Livermore, CA 94551, USA*

reactor's products containing ClN_3 pass through a drying agent (Drierite) to remove excess water before being expanded supersonically through a solenoid pulsed valve to form a molecular beam in the source chamber of the velocity map imaging[11,12] apparatus. The molecular beam is skimmed 2 cm after the nozzle and intersected perpendicularly by the focused outputs (f = 50 cm) of two counter propagating lasers. One laser (pump laser) performs the dissociation of ClN_3 and the other (probe laser) selectively ionizes the Cl photofragments in $^2P_{3/2}$ (Cl) or $^2P_{1/2}$ (Cl*) quantum-states. At 234 and 240 nm the pump and probe photons issue from the same laser beam (one-color experiment). This light was produced by sum-frequency mixing of the doubled output of a 532 nm pumped dye laser (Continuum, ND6000 operating with Rhodamine 610/640 mix around 600 nm for 234 nm generation and with DCM around 620 nm for 240 nm generation) with residual Nd:YAG-fundamental (1064 nm) (Continuum PL8020). Cl($^2P_{3/2}$) fragments at 234.076 nm are selectively ionized by 2 + 1 REMPI *via* the $^2P^o_{3/2}$ state (85 442.3 cm^{-1}). Cl*($^2P_{1/2}$) fragments are detected also in a single laser experiment by 2 + 1 REMPI *via* the $^2S_{1/2}$ state at 235.196 nm (85 035.59 cm^{-1}). For the 240 nm experiments the states and wavelengths for Cl and Cl* (2 + 1) REMPI are $^4P_{3/2}$ at 240.584 nm (83 130.90 cm^{-1}) and $^4D_{5/2}$ at 240.241 nm (84 132.26 cm^{-1}) respectively. For the 266 nm photolysis, the frequency quadrupled output of a second Nd:YAG was used and 280 nm light was generated by frequency doubling the output of a 532 nm pumped dye laser (Continuum, ND6000) at 560 nm. The ionization lasers in those two-laser experiments used the same 234/235 nm REMPI lines to detect Cl/Cl* fragments. Laser output power was about 2 mJ per pulse at 234 and 240 nm, 20 mJ at 266 nm and 10 mJ at 280 nm. It should be noted that 266 nm laser light was used unfocused.

The Cl^+ ions which formed in the repeller–extractor region of the VMI setup were mass separated in the (1 m) time of flight region of the apparatus before being detected by the 7.5 cm diameter dual MCP/phosphor position sensitive imaging detector. Ion images were recorded using a CCD/frame grabber combination (Sony XC-55/Matrix Vision PCimage SG) and Davis® imaging software. Both photolysis and ionization lasers were linearly polarized with their polarizations parallel to each other and to the detector plane in order to be able to apply the inverse Abel transformation. The velocity space in the VMI experiments was calibrated by measuring Cl and Cl* from the photolysis of Cl_2 at 355 nm.

Results

Symmetrized images of Cl and Cl* photofragments recorded following ClN_3 photolysis at 234, 240, 266 and 280 nm are presented in Fig. 1. At 234 and 240 nm dissociation wavelengths, there are two ring features in the Cl-fragment data. In Cl* images recorded at close-by photolysis wavelengths, the inner feature is barely visible. At 266 and 280 nm this feature is not present for both Cl and Cl*. For both 266 and 280 nm images, the probe laser (234 nm) also dissociates ClN_3 and contributes "background" Cl signal. Probe-only images were recorded under the same conditions and subtracted from the two-laser images. However the subtraction at 266 nm was incomplete and left a "slow ring" artifact which we do not take into account in our analysis. The inverse Abel transform was applied to the images followed by integration over angle to produce translational energy distributions and over radius to produce angular distributions.

Translational energy distributions

The energy distributions of Cl (solid line) and Cl* (dotted line) fragments following ClN_3 photodissociation at 234, 240, 266 and 280 nm are plotted in Fig. 2. The x-axis in the plots is the total (Cl plus N_3) translational energy.

The amount of energy channeled into photofragment translation is determined by conservation of energy and is (ignoring initial parent energy) the energy of the dissociating photon minus (a) the bond dissociation energy D_o and (b) the energy stored in the photoproducts electronic, vibrational and

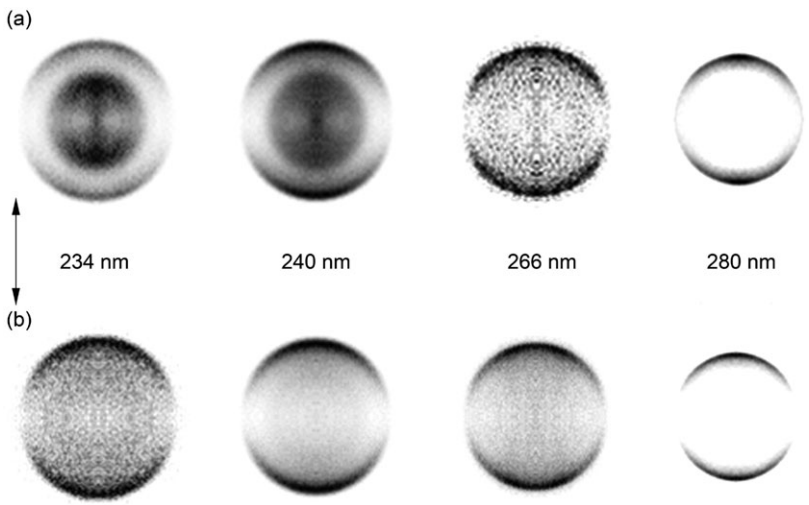

Fig. 1 Ion images at 234, 240, 266 and 280 nm: (a) Cl (top), (b) Cl* (bottom). Laser polarization is indicated by the arrow. Intensity increases from white to black. The inner feature barely visible at 266 nm is imperfectly subtracted probe laser (234 nm) signal. Images at 234, 240 and 266 nm were recorded with repeller voltage at 3 kV while that the 280 nm image was recorded at 4 kV.

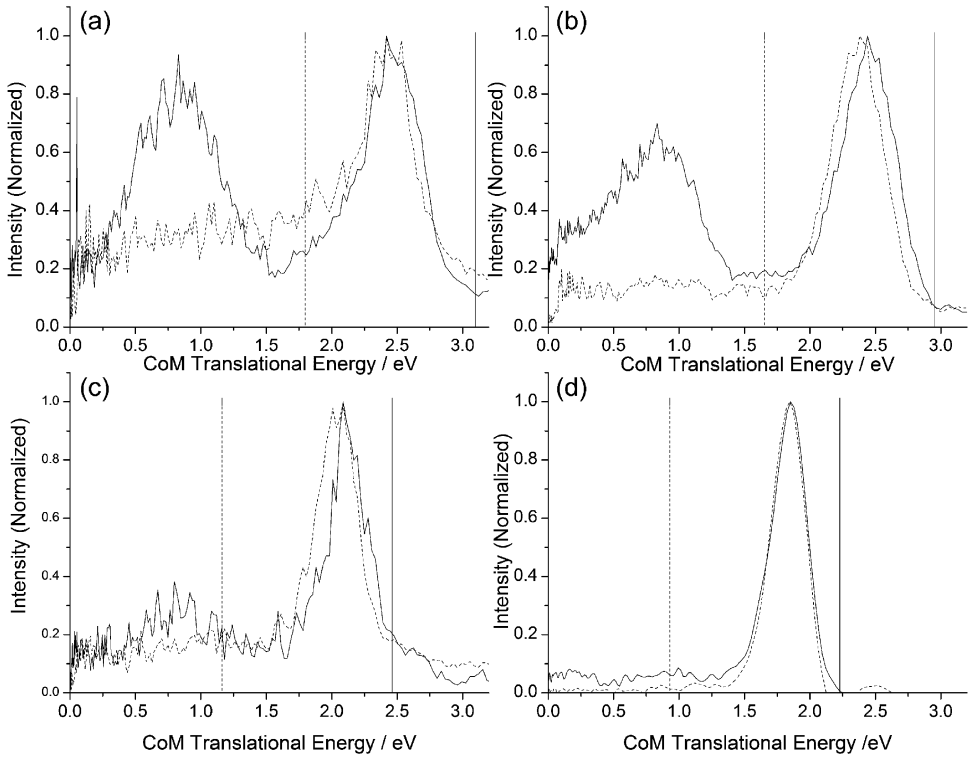

Fig. 2 Total translational energy distributions at: (a) 234 nm, (b) 240 nm, (c) 266 nm and (d) 280 nm. The solid lines are Cl and dotted ones are Cl* center-of-mass translational energy distributions. Drop-down lines mark the Cl fragments maximum translational energy if N_3 is linear (solid) or cyclic (dotted). At 266 nm experiment the signal coming from 266 nm is not as strong as that from the probe laser (234 nm), resulting in incomplete subtraction and high background signal. Similar subtraction leads to some negative intensity points in 280 nm data.

rotational degrees of freedom. The dissociation energy of the Cl–N_3 bond has been evaluated recently[2] to be 2.15 ± 0.1 eV. Assuming no internal energy is partitioned into the products, we can calculate the maximum product translational energy E_T^{MAX}, shown in Fig. 2 as a drop-down *solid* line for the Cl fragments at each wavelength. For the Cl* fragments, E_T^{MAX} will be 0.109 eV (882 cm^{-1}) lower, reflecting the spin orbit splitting energy difference.

The Cl and Cl* distributions at 234 nm agree with previous results.[2] In the Cl distribution there are two peaks, one at around 2.4 eV and another at 0.8 eV in total translational energy. We estimated the width of each peak by fitting to it a Gaussian distribution function. The FWHM for the fast peak is $\sim$0.5 eV and for the slow peak 0.7 eV. In comparison, Cl peak from Cl_2 photodissociation at 355 nm (1.02 eV total translational energy) has a FWHM of 0.06 eV. It is evident that ClN_3 photodissociation produces a distribution of internally excited N_3 fragments which cause the Cl peaks to broaden. The slow : fast area ratio between the two Cl peaks is 1.2 : 1.

In the Cl* distribution recorded at nearby wavelength, that ratio drops dramatically. The slow peak is barely visible as a ring in the image and is almost hidden in the noise of the Abel transform. To get an upper limit of its contribution, we fit a Gaussian with the characteristics of the corresponding peak of Cl (peak 0.8 eV, FWHM 0.7 eV) and got a slow : fast area ratio of 0.2 : 1. The fast Cl* distribution peaks at 2.4 eV have a width of 0.5 eV.

In the 240 nm photolysis, the Cl translational energy distribution is again bimodal peaking at 2.4 eV (FWHM 0.49 eV) and 0.84 eV (FWHM 0.75 eV). The slow : fast ratio drops to 1 : 1. Again in Cl* distribution, the slow peak is almost invisible and an upper limit of 0.2 : 1 was extracted for the slow : fast ratio. The fast Cl* peak is at 2.4 eV with FWHM of 0.4. It appears that, within experimental error, there is no significant change in the photolysis process of ClN_3 between 234 and 240 nm.

At the next photolysis wavelength studied, at 266 nm, there is significant change. We find only a single peak in the Cl distribution at 2.1 eV, with a FWHM of 0.27 eV and also a single peak in Cl* distribution at 2.04 eV with 0.29 eV FWHM. As mentioned earlier, the slow peak visible in the Cl distribution is due to 234 nm photolysis of ClN_3 signal, which was not subtracted successfully. We verified that there is no slow Cl contribution at 266 nm by fitting the unsubtracted data (not shown here) for both 234 and 266 nm slow and fast channel contributions. At 280 nm the distribution is similar to 266 with one peak at 1.84 eV (0.26 eV FWHM) for Cl and 1.83 eV (FWHM 0.25 eV) for Cl*.

Angular distribution

Integrating the 2-D image cuts over radius, we obtained the angular distributions of the Cl and Cl* fragments to which we fit the known[13] $I(\theta) = 1 + \beta P_2(\cos\theta)$ formula to extract the anisotropy parameter, β. The results are presented in Table 1 and are in agreement with previously reported work.[2,7] We did not extract an anisotropy parameter for the slow channel in the Cl* distributions because the range of this channel is not

Table 1 Total translational energy distribution peaks and widths and anisotropy parameters for the slow and fast channels of the distributions reported in Fig. 2 and in the literature, following photolysis of ClN_3 in the 234–280 nm range. The column next to the peak translational energy shows the average translational energy of the fast Cl or Cl* fragments as a percentage of available energy (E_{av}). Unless otherwise noted, the error in peaks and widths is ±0.06 eV and in percentage ±4%

Wavelength (nm)			Peak (eV)	% of E_{av}	Width (eV)	Anisotropy parameter
234	Cl	Fast	2.44	78	0.52	1.71 ± 0.1
		Slow	0.82		0.72	0.38 ± 0.1
	Cl*	Fast	2.37	79	0.54	1.72 ± 0.1
		Slow	~0.8		~0.7	—
235[a]	Cl	Fast	2.40	77	0.57	1.70 ± 0.05
		Slow	0.92			0.39 ± 0.01
	Cl*	Fast	2.31	77	0.7	1.74 ± 0.04
		Slow				0.41 ± 0.02
240	Cl	Fast	2.42	81	0.49	1.96 ± 0.1
	Cl	Slow	0.84		0.75	0.38 ± 0.1
	Cl*	Fast	2.36	81	0.40	1.91 ± 0.1
	Cl*	Slow	~0.8		~0.7	—
248[b]	Cl + Cl*	Fast	2.17 ± 0.01	79	0.45	1.75 ± 0.1
		Slow	0.74 ± 0.01		0.45	0.4 ± 0.05
266	Cl	Fast	2.12	85	0.27	1.88 ± 0.1
	Cl*	Fast	2.04	85	0.29	1.71 ± 0.1
280	Cl	Fast	1.84	81	0.26	1.85 ± 0.1
	Cl*	Fast	1.83	84	0.25	1.70 ± 0.1

[a] Data obtained from ref. 2. [b] Data obtained from ref. 7. In that experiment Cl and Cl* are not state selectively detected.

clear in the energy distributions, therefore the result would have disproportionate error bars and no useful information could be extracted from it. The fast channel β-parameter does not change significantly with wavelength, ranges from 1.7 to 1.9 and exhibits a predominantly parallel character, while the slow channel, present at 234 and 240 nm, has a more isotropic distribution and an anisotropy parameter of around 0.4 when it is present. Hansen and Wodtke[2] have observed the same anisotropy difference at 235 nm photolysis of ClN_3 (Table 1) and using Busch and Wilson's treatment,[14] they discussed two possible explanations: (a) the case of structurally different transition states (consistent with linear and cyclic N_3 formation) that give rise to different photofragment average departure angles with respect to the transition dipole moment for the slow and the fast Cl photofragments and (b) the case that slow Cl is generated by a long lived (~300 fs) intermediate. The similar anisotropy parameter values obtained by our results at 234 and 240 nm and PTS results[7] at 248 nm demonstrate that the dissociation dynamics of slow and fast Cl formation do not change significantly from 234 to 248 nm, however it is still unclear whether the more isotropic distribution of the slow Cl can be attributed to molecular geometry rearrangement during Cl–N bond breaking or to a long-lived intermediate that would allow parent molecule rotation to alter the anisotropy. The anisotropy parameters of the Cl* distributions have also parallel character, with beta ranging again from 1.7 to 1.9.

Discussion

The bimodal translational energy distributions observed here are assigned in a similar way to previous work.[2,7,8] That is, we assign the fast (or the only) peak of the translational energy distribution at each wavelength we studied, to the production of Cl and linear N_3:

$$ClN_3 + h\nu \rightarrow Cl(^2P_j) + N_3(^2\Pi_g) \quad (1)$$

The origins and widths of those peaks reveal that the linear N_3 produced by reaction (1) is ro-vibrationally excited with about 80% of the available energy appearing as translation. The average translational energy of the fast peak fragments is reported in Table 1 as % of available energy (E_{av}) for all the wavelengths in this study. Comparing results at 266 and 280 nm with those at 234 and 240 nm, it appears that N_3 internal excitation does not change significantly with wavelength or with Cl atom's spin–orbit state.

The assignment of the low translational energy peak ("slow-channel") at 234 and 240 nm continues to be the topic of current study; thus we refer to this channel as "high energy form" of N_3 or HEF-N_3 producing channel. The possibility of a direct three body dissociation yielding Cl + N_2 + N to explain it is not likely, since slow "momentum-matched" N_3 has been detected directly by PTS experiments.[7,8] Recent high-level theoretical calculations[4,5,15] on low lying excited states of N_3 predict a cyclic form of N_3, 1.35 eV above linear N_3 ground state. Previous work[2,6–8] has shown that the translational energy release in the "slow channel" is energetically consistent with formation of cyclic-N_3. This is also apparent in Fig. 2. Using D_o(Cl–N_3) of 2.15 ± 0.1 eV[2] and the theoretical predictions of the excitation energy of cyclic-N_3 with respect to linear N_3,[4] we can calculate the maximum translational energy release, E_T^{MAX}, for Cl produced with cyclic-N_3, shown as *dotted* drop-down lines in Fig. 2. The good agreement between these energetic limits and the observed translational energy distributions, now at three photolysis energies: 234,

240 nm using VMI and 248 nm using PTS, strengthen the evidence supporting the assignment of the slow-channel to cyclic-N_3 formation. Besides cyclic N_3, the only other electronically excited state of N_3 accessible in the 235–280 nm photolysis energy range is the $^4B_1$ state, theoretically predicted in the work mentioned above. As this state is spin forbidden, it is less likely that N_3 is formed in $^4B_1$ rather than in the two (linear and cyclic) spin allowed states.

The principal result from this work is the photolysis wavelength dependence of the "slow channel". Our VMI results demonstrate the existence of an energetic barrier (or possibly a minimum in a potential energy seam crossing) to "slow-Cl" production (alternatively, HEF-N_3 production) between 240 and 266 nm of ClN_3 photolysis. PTS experiments carried out at a photolysis wavelength of 248 nm using either electron impact[6,7] or synchrotron radiation photo-ionization[8] to probe the photofragments, also detect the slow peak in both Cl and N_3 translational energy distributions narrowing the barrier's possible position between 248 and 266 nm.

The collected results are shown in Fig. 3. Here, we integrated the signal intensities from imaging and PTS Cl photofragment data to obtain the "slow-Cl" branching-fraction relative to total Cl-atom production in ClN_3 photolysis at five different photolysis wavelengths. We took into account both Cl and Cl* fragment contributions in imaging experiments, weighting the Cl* contribution by the appropriate factor[16,17] due to differences in state-specific REMPI detection efficiency. From Fig. 3, one may derive a threshold for the appearance of slow-channel at 4.83 ± 0.17 eV.

Also plotted in Fig. 3 is the absorption spectrum[18] of gas-phase ClN_3 in this wavelength range. Unpublished theoretical calculations[19] indicate that the absorption system in this wavelength range is the $S_2(^1A')$–$S_0(^1A')$ system. This is substantiated by the strong parallel polarization observed in this work. The observed threshold is seen on the rising absorption edge of the $S_2(^1A')$–$S_0(^1A')$, substantially above the $S_2(^1A')$–$S_0(^1A')$ origin.

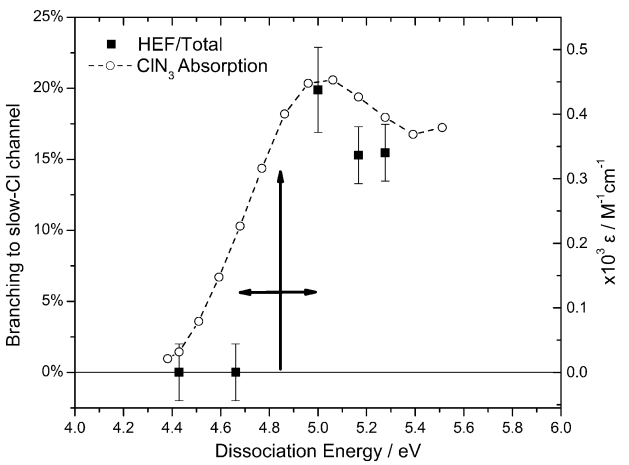

Fig. 3 Energy threshold of slow Cl production. Filled squares with error bars represent the percentage of total Cl that is slow Cl. The existence of a threshold between 4.66 and 4.99 eV is evident. The best estimated value for the threshold is 4.83 ± 0.17 eV, indicated by an upward pointing arrow. Plotted as a line is the absorption spectrum of ClN_3 in this energy region (ref. 18).

Recently, extensive theoretical calculations on the excited electronic states of HN_3 have lead to a deeper understanding of ring closing dynamics in the photochemistry of that molecule, by making careful comparisons to H-atom Rydberg tagging experiments where the photolysis wavelength was varied.[20] In that work a similar threshold for "slow-H-atom" formation was found at ~ 5.6 eV, also on the rising edge of the $S_2(^1A')$–$S_0(^1A')$ absorption. It was argued that a S_2/S_1 conical intersection, identified by theory, could lead to S_2–S_1 internal conversion allowing access to a ring-closed HN_3 isomer on the S_1 potential energy surface. The S_1 ring-closed isomer in HN_3 was located about 2.9 eV above the S_1 minimum. Here the observed threshold 4.8 eV, is similarly about 2–2.5 eV higher in energy than the red edge of the S_1 absorption of ClN_3.[21] While these comparisons can only provide incentive for new theoretical investigations of excited electronic states of the ClN_3 molecule, the similarity with the HN_3 observations and this work is striking.

We also point out in passing another interesting aspect of the experimental observations. Theory predicts a barrier to isomerization from linear to cyclic N_3 of 62.2 kcal mol^{-1} (2.70 eV). One cannot fail to notice that this barrier is suspiciously close to the energy available to the photo-products, when photolysis takes place at the slow-channel threshold.

$$E_{av} = h\nu - D_o = 4.83 - 2.15\,(\pm 0.1\text{ eV}) = 2.68\,(\pm 0.1\text{ eV}) \quad (2)$$

It is possible that this extraordinary match is purely coincidental. Nevertheless, it is suggestive of a possible mechanism for dissociation that is worth further theoretical study. Here, one would imagine that ring closure in the ClN_3 molecule takes place before the final translational energy of the recoiling Cl–N_3 half-collision pair is determined. And that the relaxation of the N_3 moiety from the ring closing saddle point into the final ring closed structure is crucial to determining the final translational energy of the slow channel.

Conclusions

We carried out velocity map imaging experiments measuring state-selectively Cl($^2P_{3/2}$) and Cl*($^2P_{1/2}$) photofragments following ClN_3 photolysis at 4 wavelengths in the 234–280 nm region of the absorption spectrum. Bimodal translational energy distributions reveal that ClN_3 photolysis at 234 and 240 nm generates N_3 in two forms: the linear and a high energy one (HEF-N_3), possibly cyclic N_3. At 266 and 280 nm only the linear form is produced. Combining those results with photofragmentation translational spectroscopy data at 248 nm, we determined the threshold for HEF-N_3 production at 4.83 ± 0.17 eV photolysis energy. A similar threshold in the HN_3 photolysis was associated recently with a ring-closed HN_3 isomer. It is an interesting coincidence that the energy available to the photofragments following ClN_3 dissociation at the threshold photon energy, matches the theoretically calculated isomerization barrier from linear- to cyclic-N_3.

In addition we find that the majority of Cl* fragments even at 234 and 240 nm are produced along with linear N_3, indicating different dynamics for this spin orbit state. However, angular distributions are similar for Cl and Cl* and also do not change significantly with wavelength. Cl + linear N_3

channel (β = 1.7–1.9) exhibits a predominantly parallel character while Cl + HEF-N_3 channel is more isotropic (β = 0.4).

Present results support previous evidence that HEF-N_3 is indeed cyclic N_3. However more work is needed to experimentally determine the structure of HEF-N_3 and theoretically explore the ring closing dynamics following ClN_3 photolysis.

Acknowledgements

Support from Air Force Office of Scientific Research (Grant. No. FA9550-04-1-0057) is gratefully acknowledged.

References

1 M. N. Glukhovtsev, H. J. Jiao and P. V. Schleyer, *Inorg. Chem.*, 1996, **35**(24), 7124–7133.
2 N. Hansen and A. M. Wodtke, *J. Phys. Chem. A*, 2003, **107**(49), 10608–10614.
3 M. Bittererova, H. Ostmark and T. Brinck, *J. Chem. Phys.*, 2002, **116**(22), 9740–9748.
4 P. Zhang, K. Morokuma and A. M. Wodtke, *J. Chem. Phys.*, 2005, **122**(1), 014106.
5 D. Babikov, P. Zhang and K. Morokuma, *J. Chem. Phys.*, 2004, **121**(14), 6743–6749.
6 A. M. Wodtke, N. Hansen, J. C. Robinson, N. E. Sveum, S. J. Goncher and D. M. Neumark, *Chem. Phys. Lett.*, 2004, **391**(4-6), 334–337.
7 N. Hansen, A. M. Wodtke, S. J. Goncher, J. C. Robinson, N. E. Sveum and D. M. Neumark, *J. Chem. Phys.*, 2005, **123**(10), 104305.
8 P. C. Samartzis, J. J. M. Lin, T. T. Ching, C. Chaudhuri, Y. T. Lee, S. H. Lee and A. M. Wodtke, *J. Chem. Phys.*, 2005, **123**(5), 051101.
9 J. M. Dyke, N. B. H. Jonathan, A. E. Lewis and A. Morris, *Mol. Phys.*, 1982, **47**(5), 1231–1240.
10 R. Tarroni and P. Tosi, *Chem. Phys. Lett.*, 2004, **389**(4–6), 274–278.
11 A. T. J. B. Eppink and D. H. Parker, *Rev. Sci. Instrum.*, 1997, **68**(9), 3477–3484.
12 M. N. R. Ashfold, N. H. Nahler, A. J. Orr-Ewing, O. P. J. Vieuxmaire, R. L. Toomes, T. N. Kitsopoulos, I. A. Garcia, D. A. Chestakov, S. M. Wu and D. H. Parker, *Phys. Chem. Chem. Phys.*, 2006, **8**(1), 26–53.
13 R. N. Zare, *Mol. Photochem.*, 1972, **4**, 1–37.
14 G. E. Busch and K. R. Wilson, *J. Chem. Phys.*, 1972, **56**(7), 3638–3654.
15 D. Babikov, B. K. Kendrick, P. Zhang and K. Morokuma, *J. Chem. Phys.*, 2005, **122**(4), 044315.
16 K. Tonokura, Y. Matsumi, M. Kawasaki, S. Tasaki and R. Bersohn, *J. Chem. Phys.*, 1992, **97**(11), 8210–8215.
17 R. Liyanage, Y. A. Yang, S. Hashimoto, R. J. Gordon and R. W. Field, *J. Chem. Phys.*, 1995, **103**(15), 6811–6814.
18 T. C. Clark and M. A. A. Clyne, *Trans. Faraday Soc.*, 1969, **65**, 2994–3004.
19 K. Morokuma, private communication.
20 J. Zhang, Y. Chen, K. Yuan, S. A. Harich, X. Wang, X. Yang, P. Zhang, Z. Wang, K. Morokuma and A. M. Wodtke, *Phys. Chem. Chem. Phys.*, 2006, **8**, 1690–1696.
21 K. Dehnicke and P. Ruschke, *Z. Naturforsch., B: Chem. Sci.*, 1978, **33**(7), 750–752.